Tectonophysics 782–783 (2020) 228426

Contents lists available at ScienceDirect

Tectonophysics

journal homepage: www.elsevier.com/locate/tecto

Seismogenic thickness of California: Implications for thermal structure and seismic hazard

Andrew V. Zuza[a,*], Wenrong Cao[b]

[a] Nevada Bureau of Mines and Geology, University of Nevada, Reno, NV 89557, United States of America
[b] Department of Geological Sciences and Engineering, University of Nevada, Reno, NV 89557, United States of America

ARTICLE INFO

Keywords:
Seismogenic thickness
D95
Crustal strength
Brittle-ductile transition
Heat flow
Seismic hazard

ABSTRACT

The seismogenic thickness of the crust, a proxy for brittle-crust thickness, is a geometric parameter related to crustal strength, seismic hazard, and the crust's thermo-mechanical nature. We use high-resolution earthquake-location data from California to construct a topographic map of the base of the seismogenic crust by calculating the depth above which 95% of seismicity (D95) is located for fixed width bins. Seismogenic thickness is highly variable, ranging from ~5 km to > 30 km, with thicker D95 values in the Great Valley-Sierra Nevada and thinner values in the Walker Lane and northern coastal California. Seismogenic thickness is inversely correlated with surface heat flow in most locations, consistent with a steady-state conductive crust, and local deviations probably reflect non-steady-state conditions related to magmatism and/or hydrothermal circulation. Such correlation suggests that, at regional scale, brittle-ductile transition (BDT) depth is mostly controlled by geothermal gradients, and the base of the seismogenic crust essentially represents a BDT isotherm (~300–350 °C for quartz-dominated lithologies). Spatial variations of D95 depths across California can be used to evaluate or constrain the locations of future seismicity, propagation direction of earthquake ruptures, and maximum depth, rupture area, and magnitude of future strike-slip earthquake events. Thicker seismogenic crust has a greater integrated strength. Seismogenic depth asperities, which represent mechanically stronger crustal patches, may focus and nucleate future earthquake events and/or impede rupture propagation.

1. Introduction

The geometry of the seismogenic crust dictates the locations and magnitudes of crustal earthquakes (Sibson, 1984, 1986; Scholz, 1990; Bonner et al., 2003; Nazareth and Hauksson, 2004; Chiarabba and De Gori, 2016; Wu et al., 2017). The seismogenic zone, which is effectively equal to the brittle-crust thickness, only occupies a fraction of total crustal thickness (e.g., Scholz, 1998). The base of the seismogenic zone correlates with the approximate location of the mostly temperature-dependent brittle-ductile transition (BDT), and the depth of this transition directly relates to the integrated yield strength of the crust (e.g., Lister and Davis, 1989; Behr and Platt, 2011, 2014; Behr and Hirth, 2014; Zuza et al., 2017).

Knowledge of any spatial variations in crustal seismogenic thickness can therefore elucidate the thermo-mechanical properties of the crust and constrain the locations of future earthquake events (e.g., Sibson, 1984, 1986; Scholz, 1990; Nazareth and Hauksson, 2004; Wu et al., 2017). Considering that thicker brittle crust is inherently stronger, assuming similar lithologies, and vice versa, these spatial thickness variations influence the possible magnitudes of such a rupture. Similarly, brittle-crust geometries may affect the geometry and length of fault rupture. The seismic moment of an earthquake depends on its rupture area, and for vertical strike-slip faults, potential rupture dimensions are partially controlled by the depth-location of the base of the seismogenic zone (Wells and Coppersmith, 1994; Console et al., 2015). Furthermore, any roughness or particular depth asperities at the base of the seismogenic crust may act as "sticking patches" that may nucleate future earthquake events (Sibson, 1984).

Given the potential influence of seismogenic crust thickness on earthquake locations and magnitudes, a detailed understanding of spatially varying seismogenic thickness can aid seismic hazard evaluation (Bonner et al., 2003; Nazareth and Hauksson, 2004; Chiarabba and De Gori, 2016; Wu et al., 2017). The vertical position of the BDT in a column of rock is affected by a variety of factors, including geothermal gradient, lithology, water content, and strain rate (Sibson, 1982; Hirth and Beeler, 2015). Here we take the approach of using high-resolution earthquake-location data to constrain the thickness of the seismogenic crust as a proxy for BDT depths (Williams, 1996;

* Corresponding author.
E-mail addresses: azuza@unr.edu (A.V. Zuza), wenrongc@unr.edu (W. Cao).

https://doi.org/10.1016/j.tecto.2020.228426
Received 23 October 2019; Received in revised form 25 February 2020; Accepted 26 March 2020
Available online 04 April 2020

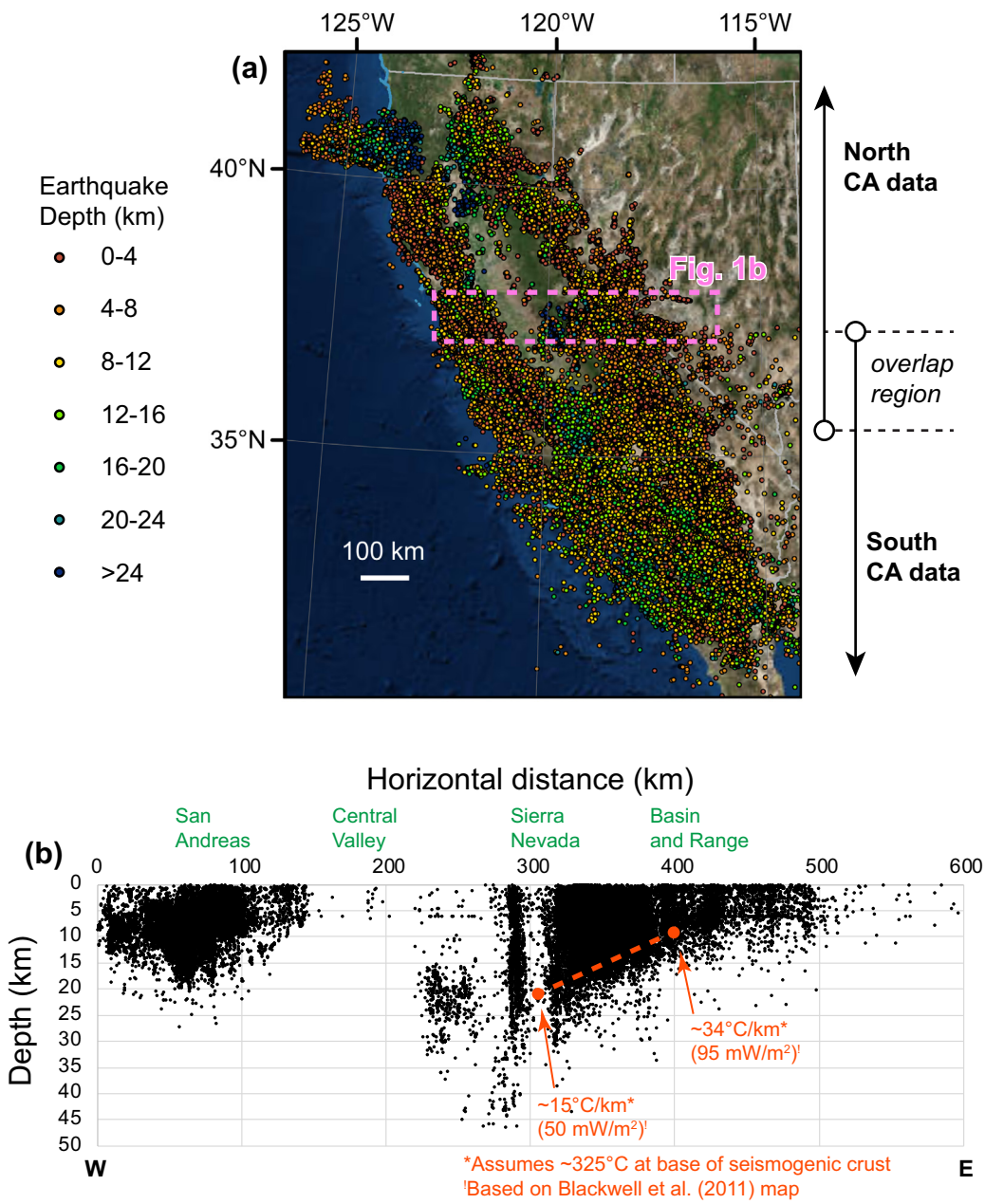

Fig. 1. (a) Map of earthquake epicenters around California used in this study, color-coded by depth. Pink box outlines swath profile shown in (b). Data for northern California from Schaff and Waldhauser (2005) and Waldhauser and Schaff (2008); data from southern California from Hauksson et al. (2012). Note overlapping zone between datasets, which was investigated to test potential biases between data in Fig. 4. (b) ~100-km-wide swatch profile across California, demonstrating west-east variations in seismogenic thickness across the study area. Note the systematic shallowing of seismicity moving from the Sierra Nevada to the Basin and Range that mirrors a similar decrease in observed surface heat flow (Blackwell et al., 2011). (For interpretation of the references to color in this figure legend, the reader is referred to the web version of this article.)

Nazareth and Hauksson, 2004; Chiarabba and De Gori, 2016), which can then be used to make first-order estimates for spatial variations of crustal strength.

Using relocated earthquake datasets for California (Schaff and Waldhauser, 2005; Lin et al., 2007; Waldhauser and Schaff, 2008; Hauksson et al., 2012) we constructed a seismogenic thickness map of California, USA, and the immediate surrounding regions. This map demonstates the spatially varying depth of the frictional stability transition (FST), which we assume is equivalent to the BDT. Accordingly, we show the significant heterogeneity of brittle-crust thickness across California. Crustal thermal structure mostly controls this diversity, but rock types, water content, and strain rates may also affect seismogenic thickness. These maps can improve our knowledge of earthquake hazard models including potential rupture areas for fault zones and tests of existing fault-hazard models against earthquake distributions. Ultimately, these geometric parameters can be incorporated into continental tectonics and physics-based earthquake models (e.g., Bird and Kong, 1994; Console et al., 2015; Schultz et al., 2018; Ceferino et al., 2019).

2. Rationale and methods

Earthquake hypocenters should primarily be confined to the seismogenic crust above the BDT, or FST, in the frictional deformation regime (Fig. 2a and b). The transition from brittle-frictional regime to the ductile-viscous regime probably occurs over a broad zone of several kilometers, across a zone of velocity-strengthening deformation that produces little-to-no earthquakes (e.g., Scholz, 1988). Herein, we make the simplifying assumption that this transition approximately occurs at the point (e.g., Sibson, 1986) at which frictional and power-law ductile yield strength curves intersect, which corresponds approximately to the thickness of the seismogenic crust (Fig. 2a). This vertical position of the BDT is controlled by depth at which dislocation creep becomes the dominant deformational mechanism when temperatures are high enough to allow viscous flow of the constituent rock column (e.g., Goetze and Evans, 1979; Sibson, 1982, 1984; Scholz, 1998) (Fig. 2a). The temperature at which this transition occurs depends on rock composition, water content, and strain rate, and the corresponding depth is related to geothermal gradient (Sibson, 1974, 1982, 1984; Hirth and

Beeler, 2015; Hauksson and Meier, 2018). Viscous rock flow is assumed to follow a power-law stress-strain relationship, and for quartz-dominated lithologies, quartz plasticity occurs at 300–350 °C for typical geologic strain rates. At a reasonable continental geothermal gradient of ~25 °C km^{-1}, this corresponds to a BDT depth of 12–14 km (e.g., Behr and Platt, 2014). Viscous flow of feldspathic or dioritic compositions requires higher temperatures, resulting in a deeper BDT and therefore stronger crust for a given thickness.

Yield strength envelopes developed for the crust schematically illustrate the stress at which the crust deforms plastically (Goetze and Evans, 1979), and the depth location of the BDT ultimately controls the integrated strength of the crust (Fig. 2) (Lister and Davis, 1989; Jackson et al., 2008). A deeper BDT yields a larger integrated yield strength magnitude, and vice versa. This is illustrated in a plot of integrated yield strength of the crust as a function of geothermal gradient, varying strain rates from 10^{-17} s^{-1} to 10^{-14} s^{-1}, constructed using the RHEOL_GUI script of Montesi and Leete (2018) and quartzite flow laws of Hirth et al. (2001) (Fig. 2c). These values are approximate as variations in strain rate, lithology, and water content are not considered. However, the plot highlights how doubling the geothermal gradient more than halves the integrated strength of the crust (Fig. 2c).

Given the strong temperature-dependence of BDT depths, heat flow data can be used to invert for thermal structure and ultimately BDT depths assuming steady-state conditions. This method can be used to construct a theoretical yield envelopes. However, complications arising from non-steady state conductive versus convective and advective cooling, parameter and rock-type variability (e.g., grain size, lithology, water content, and strain rate), and a potentially diffuse BDT (Carter and Tsenn, 1987; Pec et al., 2016) make these estimates imprecise. Instead, here we use the depth distribution of earthquakes to directly constrain the geometry of the seismogenic crust, which we argue is a reasonable proxy for BDT depths.

For this study, we compiled the latest publicly available relocated earthquake datasets for California, available on the Southern California Earthquake Data Center and Lamont-Doherty Earth Observatory websites (Schaff and Waldhauser, 2005; Lin et al., 2007; Waldhauser and Schaff, 2008; Hauksson et al., 2012) (Fig. 1). Earthquake location data from northern California encompasses events from 1984 to 2011 that were relocated by waveform cross correlation and double-difference methods (Schaff and Waldhauser, 2005; Waldhauser and Schaff, 2008). Reported vertical relative depth precision is < 0.7 km at 95% confidence. Earthquake events from 1981 to 2011 are compiled in the southern California earthquake database of Lin et al. (2007) and Hauksson et al. (2012) with relative errors of < 1.25 km at 90% confidence. Together, the data includes > 10^6 events (Fig. 1).

The depths of relocated earthquake hypocenters vary significantly across California (CA), specifically the maximum depth of seismicity (Fig. 1). For example, an east-west profile across California shows concentrations of earthquakes along the San Andreas fault, an obvious lack of seismicity across the Central Valley and western Sierra Nevada, and then renewed seismicity going into the Basin and Range extensional province (Fig. 1b). Furthermore, there is a clear shallowing of the base of maximum seismicity depth moving east from the Sierra Nevada into the Basin and Range (Fig. 1b). These qualitative variations imply similar variations in seismogenic thickness across California.

The goal of this study was to construct a seismogenic thickness map across California using the aforementioned relocated earthquake database. We generated fixed width bins across the study area and evaluated the depth above which 95% crustal seismicity occurs (D95) in each bin (Sibson, 1982) (Figs. 2b and 3). We excluded bins with < 10 earthquake events. Fig. 2b shows data from one example bin, demonstrating how the D95 depth is located below 95% of the seismicity and at a natural inflection point in a cumulative earthquake-depth distribution. Uncertainty of the D95 values (Fig. 3) was calculated by generating matrices of D91 and D99 and averaging the variation from D95, which captures the inflection point of the cumulative earthquake-depth distribution (Fig. 2b).

There are two caveats to this methodology: (1) limited temporal sampling of the data and (2) merging of two separate datasets from northern and southern California. Limited temporal sampling of the data, which spans ~30 years of events, could introduce biases because it was an order of magnitude shorter than typical fault recurrence intervals (e.g., Parsons, 2008; Scharer et al., 2010). Seismogenic depth does not vary significantly or systematically for the first half (1981–1996) versus the second half (1997–2011) of the relocated earthquake catalog, with average differences of 1.4 km (Supplemental Fig. 1). Therefore, we predict the time bias is minimal but emphasize that in the future, evaluation of longer timespan datasets may explore crustal seismicity and seismogenic thickness over the seismic cycle.

The use of two different databases for northern (Schaff and Waldhauser, 2005; Waldhauser and Schaff, 2008) and southern (Hauksson et al., 2012) California, which involved different methods for earthquake relocation, could affect the final seismogenic thickness maps. In particular, the absolute depth of relocated seismicity may vary between the two datasets based on the different velocity models. The two datasets overlap in central California (Fig. 1a), and therefore we first explored and compared the seismogenic thickness derived from each dataset independently.

For this data verification, we only used bins with > 100 earthquakes and used a 22.5-km-wide fixed bin width. D95 values were generated using just the northern California data, just the southern California data, and the combined datasets (Fig. 4). Seismogenic thickness maps made from the northern and southern California datasets resulted in overlapping D95 values that were mostly within ~5 km of each other (Fig. 4a). There was no systematic difference between the two datasets and the merged dataset, as observed in Fig. 4b. The mean difference between the two datasets was −0.7 km, and it appears that the southern California data potentially resulted in slightly deeper D95 values. We attribute this minor difference to the fact that the southern California dataset involved fewer relocated earthquake events, and less events per bin, than the northern California data. The uppermost crust contains most of the seismicity, and therefore more events per bin could result in an upward shift of the D95 value. In summary, we do not believe that these different datasets significantly or systematically affect our seismogenic thickness map results because (1) the two datasets individually generated very similar seismogenic thickness maps, (2) mean variations between the two datasets were small at −0.7 km, and (3) the broad seismogenic thickness pattern does not change abruptly moving from south to north. However, we note that the northern California dataset had more earthquakes per bin, which may result in a bias toward marginally thinner seismogenic thickness estimates.

With these caveats in mind, seismogenic thickness maps were constructed and filtered with a rotationally symmetric Gaussian lowpass filter (size 2, standard deviation 2), which smoothed sharp D95 gradients and did not change the overall structure. Original unfiltered maps are shown in Supplemental Fig. 2. Varying bin widths between 20 km and 25 km produced nearly identical maps (Fig. 3). The choice of bin width involves a tradeoff between spatial D95 resolution and having enough earthquakes per bin to obtain reliable results. In addition the number of earthquakes per bin was plotted (N in Fig. 3), which allowed for qualitative evaluation of confidence for a given bin. That is, when $N \geq 100$, the calculated D95 value is more robust because there are more events constraining the seismogenic thickness of the crustal column. Note that regions with low N values (i.e., $N < \sim 25$) are probably relatively strong and/or less strained because they are not producing seismicity, and indeed bins with no calculated D95 (i.e., blank bins due to $N < 10$ events) are adjacent to the greatest seismogenic/brittle-crust thicknesses (Fig. 3).

3. Results

Filtered D95 maps are shown in Fig. 3. Note that most of the bins

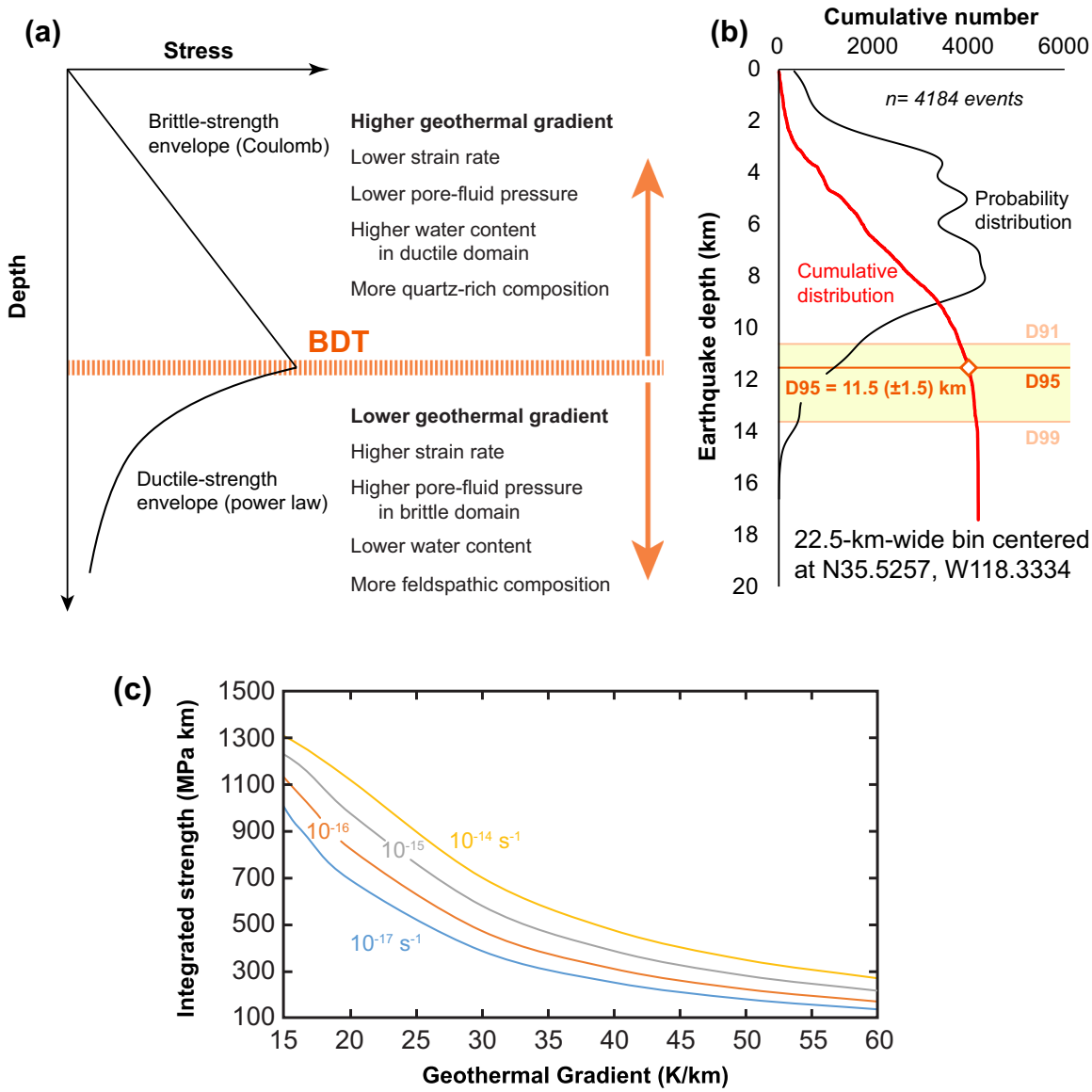

Fig. 2. (a) Theoretical yield strength envelopes for the crust, including factors that can move the brittle-ductile transition (BDT) up or down (adapted from Sibson, 1984). (b) Example of earthquake depth distribution from one 25-km-wide bin (centered at N35.5257, W118.3334), showing cumulative and probability distributions. For this example, D91, D95, and D99 values, are calculated, and the average spread over this range is the uncertainty added to the reported D95 value. Note that D95 corresponds to the approximate BDT depth in (a). (c) Integrated, strength of the crust as a function of geothermal gradient, contoured by strain rate, calculated via the RHEOL_GUI code of Montesi and Leete (2018) using quartz flow laws of Hirth et al. (2001).

had > 100 earthquake events, although smaller bins (i.e., 20 km width) predictably had more bins with no, or fewer, earthquakes than larger bins (i.e., 25 km width). Our uncertainty calculations demonstrates variations of < 5 km for most of the study area, as shown in the predominance of red-orange colors in the lower panels of Fig. 3. Importantly there is no spatial tendency to the uncertainty magnitudes (Fig. 3). That is, particular regions do not have larger uncertainties than others, and thus the results do not appear to involve any systematic spatial biases. There is no strong correlation between D95 depth and uncertainty magnitude for a given bin (see Supplemental Fig. 3). Although the determined uncertainty values (i.e., mostly ≤5 km) are significantly greater than the vertical uncertainties for each individual hypocenter in the studied catalogs (i.e., < 1.25 km), we favor this conservative larger uncertainty evaluation because it reflects geologic irregularity contained within a single bin, a diffuse BDT, and the progressive downward event distribution taper of seismicity as observed in Fig. 2b.

All three bin-width D95 maps show the same gross structure (Fig. 3). There are D95 maxima (i.e., bluer colors; D95 > 20 km) in the Central Valley and Sierra Nevada regions, in the borderland region of southern California, and north of the Mendocino triple junction in northern California (Fig. 3). We note that the northernmost D95 maximum is strongly influenced by subduction in the Cascadia arc. An east-west profile of earthquake depths reveals the east-subducting slab geometry at depths > 20 km (Fig. 5), and we accordingly do not discuss the apparent thicker seismogenic crust in the northwest portion of the study area. D95 minima are concentrated along the west coast of central and northern California where the San Andreas fault splits into several parallel fault strands and the eastern study area, coincident with the Walker Lane-Eastern California Shear Zone and Basin and Range (Fig. 3).

The Mojave region, bounded respectively by the San Andreas and Garlock faults to the southwest and north, shows average D95 values of 10–12 km (Fig. 3), which overlaps estimates from Williams (1996). Behr and Hirth (2014) document recent (i.e., 7 to 1 Ma) mantle xenoliths from Mojave that record ~900 °C at ~30 km depth, suggesting a

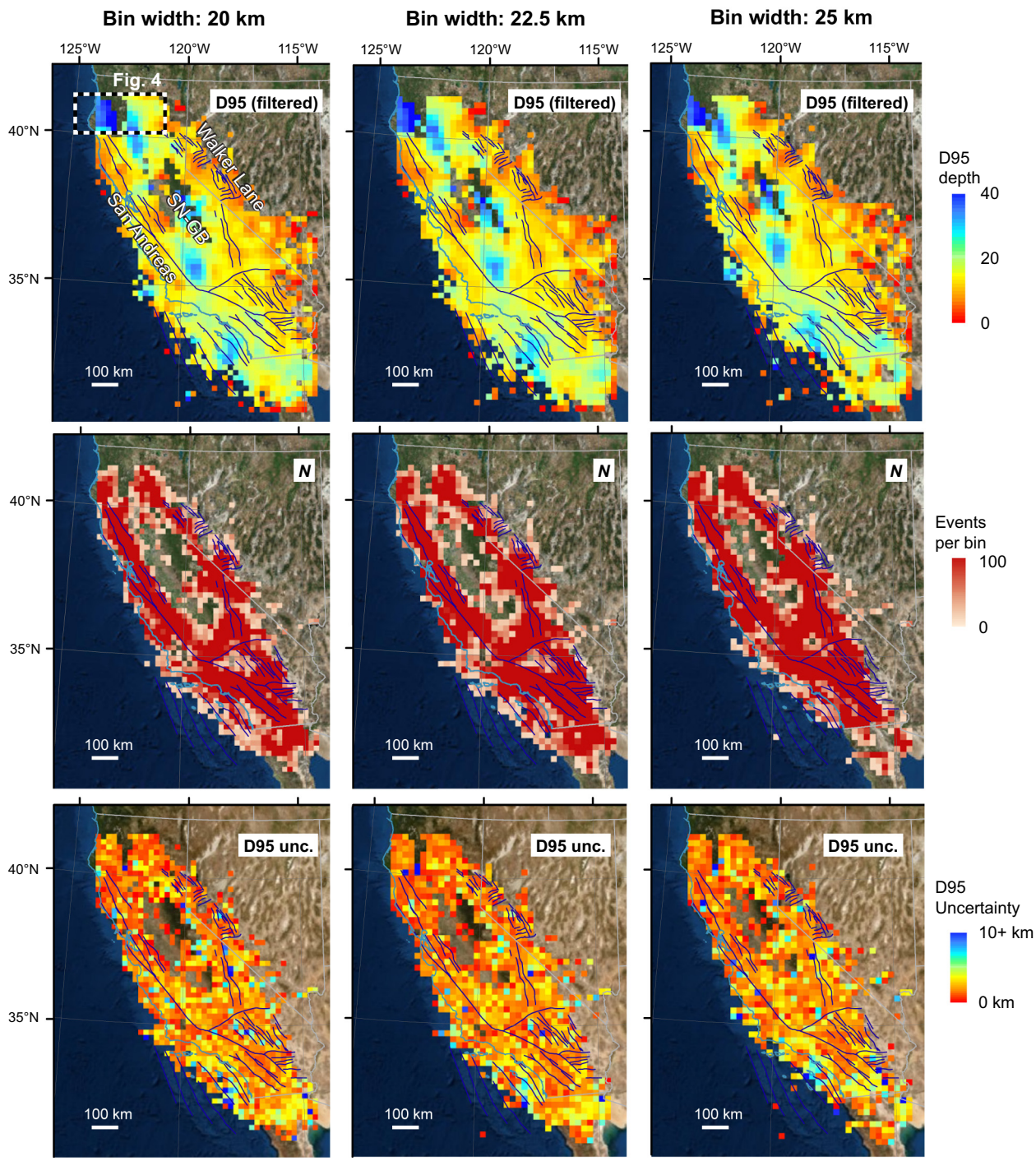

Fig. 3. D95 maps, number of earthquakes per bin (N), and associated uncertainties (unc.; average variation between D91 and D99 against D95) for different bin widths: (a) 25 km, (b) 22.5 km, and (c) 20 km. Black and white outline in the top-left panel shows east-west swatch profile of seismicity across the southernmost Cascadia subduction zone shown in Fig. 5.

bulk (paleo)geothermal gradient of 30 °C km^{-1}. Our observed 10–12 km D95 values here suggest a similar geothermal gradient of 27–33 °C km^{-1}, assuming that the base of the seismogenic crust equals approximately the temperature of quartz plasticity at ~325 °C as discussed below.

4. Discussion

4.1. Seismogenic thickness versus strain rate and heat flow

Here we compare the seismogenic thickness maps against strain rate (Kreemer et al., 2012) and surface heat flux (Blackwell et al., 2011). Theoretical strength envelopes for the crust based on power law rheology suggest that BDT depths should correlate with strain rate and anticorrelate with heat flow (e.g., Sibson, 1984). This relationships can be viewed in Fig. 2c. At a constant geothermal gradient, an order of magnitude faster strain rate yields an integrated strength increase of ~100 MPa km, whereas at a fixed strain rate, halving the thermal gradient results in more than doubling integrated strength values. That said, thinner brittle crust should be weaker (Fig. 2), and may be expected to deform more rapidly and thus have a higher strain rate. Another complication is that strain rates may vary vertically, depending

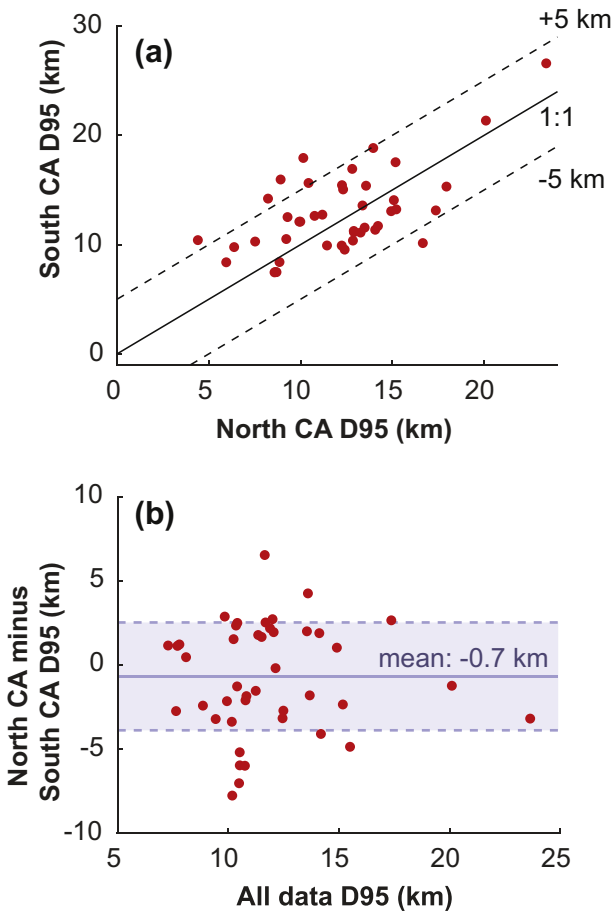

Fig. 4. Examination of northern (Schaff and Waldhauser, 2005; Waldhauser and Schaff, 2008) versus southern (Hauksson et al., 2012) California relocated earthquake datasets for latitudes where the data spatially overlap (see Fig. 1a). (a) D95 depth for the northern CA data plotted against the southern CA data. Most data plots within 5 km of the 1:1 reference line. (b) The difference between northern and southern CA D95 data plotted against the D95 value derived from the merged dataset with all earthquake locations. Average difference is −0.7 km (purple shading is 1 standard deviation). This plot shows no systematic variation of dataset difference with D95 depth. Both plots suggest that the southern CA data can yield slightly deeper D95 values. This could be caused by the fewer relocated earthquakes, and thus fewer per bin in the southern CA data, which results in a deeper D95 depth as discussed in the text.

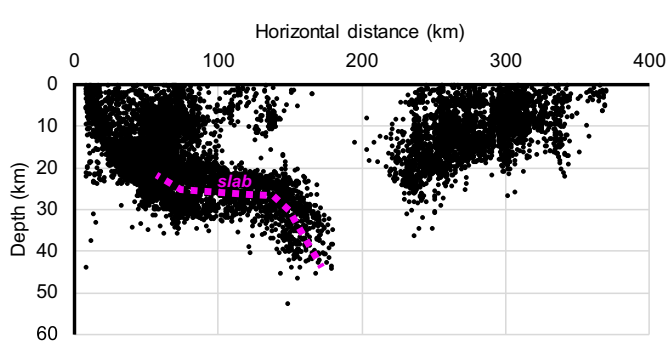

Fig. 5. ~100-km-wide swatch profile across northern California and the southernmost extent of the Cascadia subduction zone (location in top-left panel of Fig. 3) demonstrating obvious influence of the eastward subducting plate on seismicity. The apparently deeper calculated D95 depths in this region are artifacts caused by the deeper subducting slab (pink dashed line highlights trend), and therefore do not reflect the properties of the upper brittle continental crust.

on the degree of coupling between the upper and middle crust.

There is no correlation between strain rate and D95 depths based on qualitative visual inspection of Fig. 6a, and their Spearman's rank correlation coefficient, ρ, confirms a lack of correlation at 0.05 (Supplemental Fig. 4). High strain zones in California-Nevada are focused along the San Andreas fault and in the Walker Lane-Eastern California Shear Zone, which have strain rates > 10^{-15} s^{-1} compared to lower rates elsewhere of ~10^{-16} s^{-1} (Fig. 6a). There is no consistent pattern of strain rate versus seismogenic thickness along the San Andreas fault—the high-strain plate-boundary fault is essentially invisible in the D95 maps—but we do observe thinner seismogenic crust thickness around the relatively high strain-rate Walker Lane (Fig. 6a). The thinner seismogenic crust near the Walker Lane-western Great Basin also correlates with higher heat flow and geothermal gradients (e.g., Fig. 1b). Together, these observations suggest that strain rate does not strongly control the seismogenic thickness of the western US, and fast strain rates do not focus specifically on thinner seismogenic crust.

There should exist a strong dependence of BDT depth on crustal thermal structure (Fig. 2), and seismogenic crust thickness is expected to inversely correlate with surface heat flow, such that thinner seismogenic crust implies higher surface heat flow and hotter geothermal gradients. For example, we note that in an earthquake-depth profile across the Sierra Nevada in Fig. 1b, earthquakes occur 2× deeper under the Sierra Nevada than the western Basin and Range. Assuming the D95 earthquake cutoff corresponds to ~325 °C, these depths correspond to thermal gradients that vary by a factor of two, ~15 °C km^{-1} and ~34 °C km^{-1}, respectively (Fig. 1b). Observed surface heat flow estimates for these two locations also vary by nearly a factor of two: ~50 mW m^{-2} and ~95 mW m^{-2} respectively (Fig. 1b) (Blackwell et al., 2011). This example demonstrates how D95 depth and the thermal structure of the crust are closely related.

Our data shows that there is a negative correlation between heat flow (Fig. 7) and D95 depth: ρ = −0.26 (Supplemental Fig. 4). To evaluate this relationship, and any spatial controls on this negative correlation, we applied two methods: (1) estimation of the base of the seismogenic crust using surface heat flow observations to compare against D95 maps, and (2) inversion of D95 depths to predict apparent surface heat flow assuming a steady state conductive crust. Both methods assume that D95 depth, z_{D95}, equals the BDT depth at the temperature of quartz plasticity, T_q. Therefore, the geothermal gradient, Γ, of a bin equals the difference of T_q and surface temperatures, T_s, divided by the D95 or BDT depth. To relate Γ to surface heatflux, Q, we employed the simplified expression presented by Doser and Kanamori (1986):

$$T(z) = T_s + \frac{Qz}{k} + \frac{Az^2}{2k} \tag{1}$$

where $T(z)$ is temperature at depth z, k is thermal diffusivity, and A is radiogenic heat production. This can be rearranged to

$$\frac{T_q - T_s}{z_{D95}} = \Gamma_q = \frac{Q}{k} + \frac{Az_{D95}}{2k} \tag{2a}$$

$$Q = \Gamma_q k - \frac{1}{2} A z_{D95} \tag{2b}$$

$$z_{D95} = f(Q) \tag{2c}$$

where Γ_q is the geothermal gradient estimated specifically from z_{D95} and T_q. Using reasonable values of $A = 1.6 \times 10^{-6}$ W m^{-3}, $k = 3.33$ W m^{-1} K^{-1}, T_q of either 325 °C or 375 °C to approximate a range from quartz-rich to more multiphase feldspathic rheology respectively, and $T_s = 15$ °C (e.g., Doser and Kanamori, 1986), Q or z_{D95} can be solved if one of them is known via Eq. (2b) or (2c). In the above example about Sierra Nevada seismicity and heat flow, the apparent geothermal gradients estimated from maximum seismicity depths (i.e., ~15 °C km^{-1} and ~34 °C km^{-1} for the Sierra Nevada and Basin and Range, respectively) can be inverted for apparent surface heat flow

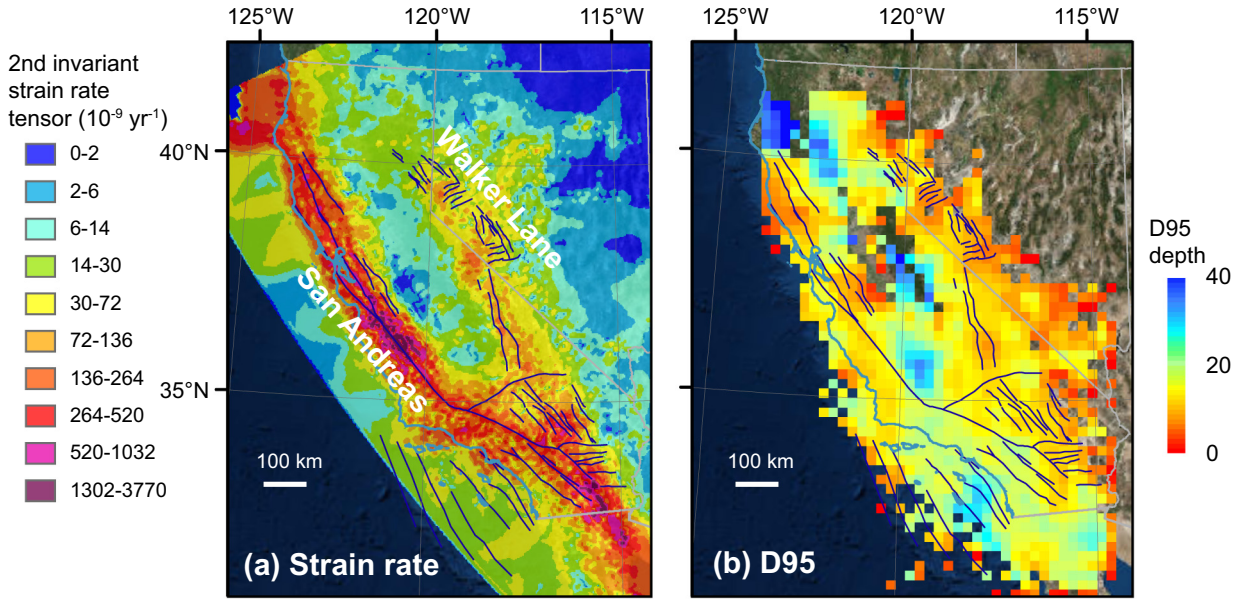

Fig. 6. Comparison of (a) strain rate (Kreemer et al., 2012) versus (b) D95 depth (22.5 km, bins) across California. Note that the higher strain rate associated with the San Andreas and Walker Lane regions does not correlate with zones of thinnest D95 values.

using Eq. (2b), which yields values of 33 mW m^{-2} and 106 mW m^{-2} respectively (Fig. 1b). These values are comparable to Blackwell et al. (2011) heat flow estimates of ~50 mW m^{-2} and ~95 mW m^{-2} respectively (Fig. 1b), and the relative differences are similar.

Near-surface hydrology and other non-steady-state processes can significantly impact continental scale heat flow maps, such as the Blackwell et al. (2011) data (Fig. 7a). Heat flow values less than ~35 mW m^{-2} or greater than ~90 mW m^{-2} almost certainly reflect these non-steady-state conditions, and the following comparison of heat flow data to D95 maps, as discussed below, highlights these particulars. We use heat flow data (Blackwell et al., 2011) to predict expected BDT depths based on Eq. (2) above. That is, given an observed surface heat flow value, we can estimate the depth at which temperature exceeds T_q, which should represent the base of the seismogenic crust. The resulting map is in the Supplemental Fig. 5, and Fig. 7b shows the difference between D95 depths and BDT depths estimated from surface heat flow data; the darkest blue and brown colors show differences exceeding 5 km. Most of these values are similar (i.e., differences < 5 km), with an average depth difference between these two maps of −0.9 km (± 5 km; 1σ) (Fig. 7b) (Supplemental Fig. 5).

Alternatively, maps of apparent heat flow constructed from D95 depths, Eq. (2b), compared against the surface heat flow map of Blackwell et al. (2011) reveals broadly similar structures (Fig. 7). That is, lower heat flow values in the Central Valley, Sierra Nevada, and southern borderland region of southern California (< 50 mW m^{-2}) and heat flux highs along the western parts of Nevada and Salton Trough (≥100 mW m^{-2}) (Fig. 7).

The fact that both comparisons of heat flow versus D95 maps reveal similar patterns confirms that thermal structure strongly controls seismogenic thickness. Fine-tuning of the heat flow inversion, such as spatially varying heat production and diffusivity parameters, could produce more correlative maps, but that is not the point of this comparison. Rather, a first order inversion of heat flow data reproduces the gross structure of the D95, seismogenic thickness maps. That said, there are several notable inconsistencies between D95 maps and heat flow data. Heat flow-based BDT estimates in the southern borderland region of southern California are shallower than observed D95 depths (Fig. 7b). Somewhat elevated heat flux values in the borderland region of southern California of ~60–80 mW m^{-2} (Lee and Henyey, 1975; Blackwell et al., 2011) suggests a thinner brittle crust than observed in D95 maps (Fig. 7). These differences may be caused by a competition of potential thermal blanketing of this region by 2–5+ km of sediments affecting the thermal structure (e.g., Nazareth and Clayton, 2003; Łuszczak et al., 2017) and a more mafic composition of the borderlands (Mooney and Weaver, 1989), supported by Vp/Vs ratios > 1.9 (Lowry and Pérez-Gussinyé, 2011), that would shift the BDT depth deeper than more felsic crust with similar heat flow values. Furthermore, the oceanic crust affiliation of the borderlands implies little crustal hydration and associated weakening, which could result in deeper-than-expected earthquakes. Given that hydration state can affect quartz abundance via feldspar breakdown (e.g., Ma and Lowry, 2017), lower quartz contents may be enhanced due to the lack of hydration compared to the continental crust to the east.

In addition, extremely elevated heat flow values in the Salton Tough region predict thinner brittle crust than the D95 maps suggest (Figs. 3 and 7). The Salton Trough has the highest heat flow in California, with values > 100–150 mW m^{-2}, up to 600 mW m^{-2} (Onderdonk et al., 2011; Procesi et al., 2019) (Fig. 7a). These extremely high heat flow values suggest a significant non-conductive component, in addition to heat conduction (Procesi et al., 2019), implying non-steady-state conditions driven by active rifting and intrusions (Lachenbruch et al., 1985; Shinevar et al., 2018). Although the D95-dervied heat flow maps show the Salton Trough as hot, it is significantly less of a high-heat flow anomaly than the observed heat flow data shows (Fig. 6a) (Blackwell et al., 2011). These differences probably arise because of these aforementioned non-steady-state conditions.

In northernmost California, D95 depths are deeper than heat flow would predict, which is caused by the previously discussed subducting slab (Fig. 5). There are also regions of the Great Valley that either have deeper or shallower D95 depths than heat flow values predict (Fig. 7). Overall, the Great Valley has a relatively thick brittle crust with relatively less seismicity (Fig. 3). Therefore, the patches where heat flow data predicts deeper BDT depths than observed in the D95 maps (brown bins in Fig. 7b) are probably caused by relatively fewer earthquakes in these crustal columns resulting in an underestimation of D95 depths.

In the southern Great Valley, D95 depths are deeper than what relatively moderate heat flow values predict (Fig. 7). Nazareth and Hauksson (2004) similarly observed some of the thickest brittle crust in the southern Great Valley (southern San Jaoquin Valley) in the earthquake-depth data. Because this region is covered by thick sediments in

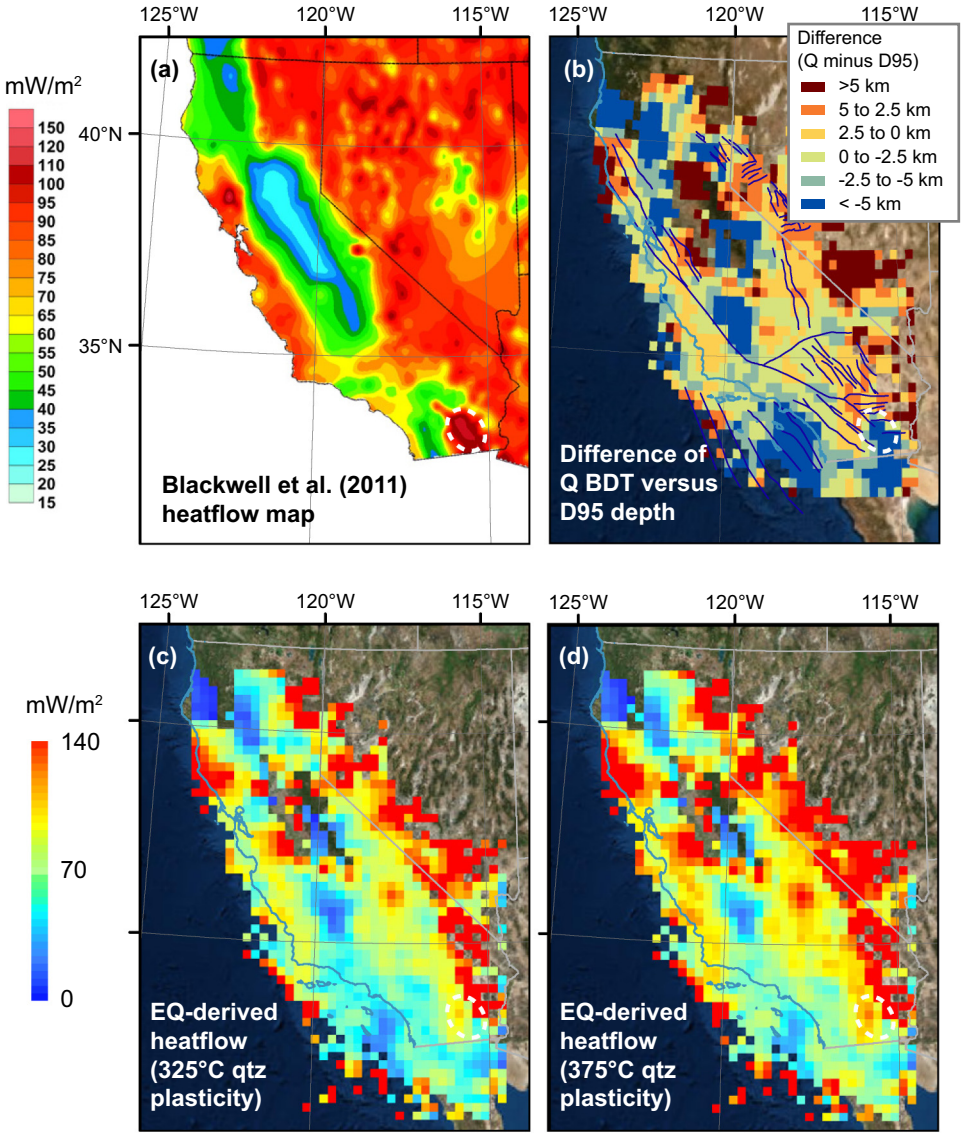

Fig. 7. Comparison of D95 and surface heat flow. (a) Blackwell et al. (2011) surface heat flow map at same projection and scale as other maps in this study. (b) Difference between heat-flow-derived estimates (Q) of brittle-ductile transition (BDT) depth (~325 °C) and earthquake-derived D95 depth maps from this study. Note that that dark blue and dark brown represent absolute differences ≥5 km, with dark blue values indicating that Q-based estimates suggest a thinner brittle crust than earthquake-based D95 estimates, and vice versa. (c-d) D95-derived estimates of apparent surface heat flow (22.5 km bins) assuming D95 depth approximately represents the quartz plasticity isotherm at (c) ~325 °C or (d) ~375 °C. In all panels, white oval highlights the Salton Trough. See text for methods and discussion. (For interpretation of the references to color in this figure legend, the reader is referred to the web version of this article.)

the Great Valley, there is a complex interaction between sedimentary cover, underlying bedrock, and water circulation that affects heat flow estimated at the surface (e.g., Harrison and Bé, 1983; Braun et al., 2016; Łuszczak et al., 2017), including a tradeoff between lower conductivity sedimentary cover and apparent conductivity increases based on water/heat convection. Herein, we have only assumed constant thermal conductivity. If we treat the D95 depth as a permissible estimate for the base of the brittle crust, then it follows that the surface heat flow values are locally and superficially elevated in the southern Great Valley (green colors in Fig. 7a) relative to the rest of the valley (blue colors in Fig. 7a), such that they predict a shallower BDT than what is observed. Water circulation is particularly effective at increasing the apparent surface heat flux (e.g., Cao et al., 2019), and a small increase of diffusivity from 3.33 to 4 W m^{-1} K^{-1} increases estimated surface heat flux by > 15 mW m^{-2} and calculated BDT depths by > 2 km. Similar to the southern California borderlands, the southern Great Valley shows show higher Vp/Vs ratios (> 1.9) relative to much of California (< 1.8) (Lowry and Pérez-Gussinyé, 2011), which may indicate more mafic crust with less crustal quartz content in these regions, thus making the seismogenic crust thicker. We do not further interpret what causes these discrepancies, acknowledging it probably involves temporal and spatial variations in the basin's thermal history (e.g., Harrison and Bé, 1983), its underlying rock composition (e.g., Oskin et al., 2016), and ground water circulation.

These examples highlight how surface heat flow data may not reliably predict BDT depth values. Accordingly, D95-based estimates of brittle-crust thickness may see through these types of complications that affect heat flow datasets. This can provide more information on the bulk thermal structure of the upper crust, especially when integrated with all available datasets including heat flow observations and Moho temperature (e.g., Schutt et al., 2018).

4.2. Constraints for future seismicity

Similar seismogenic thickness maps have been constructed for Taiwan and Italy (Chiarabba and De Gori, 2016; Wu et al., 2017) and smaller regions of California using older earthquake datasets (Bonner et al., 2003; Nazareth and Hauksson, 2004; Shinevar et al., 2018). The seismogenic thickness map of all of California presented in this study using updated high-resolution earthquake-location datasets provides insight into the mechanical properties of the crust through which major earthquake-producing faults exist and rupture. For example, the maps highlight how the San Andreas fault traverses 100s of km through highly variable brittle-crust thickness (Fig. 8), and similarly, major historical earthquake ruptures along the fault cut through variable thickness brittle crust. Both the 1857 Fort Tejon and 1906 San Francisco

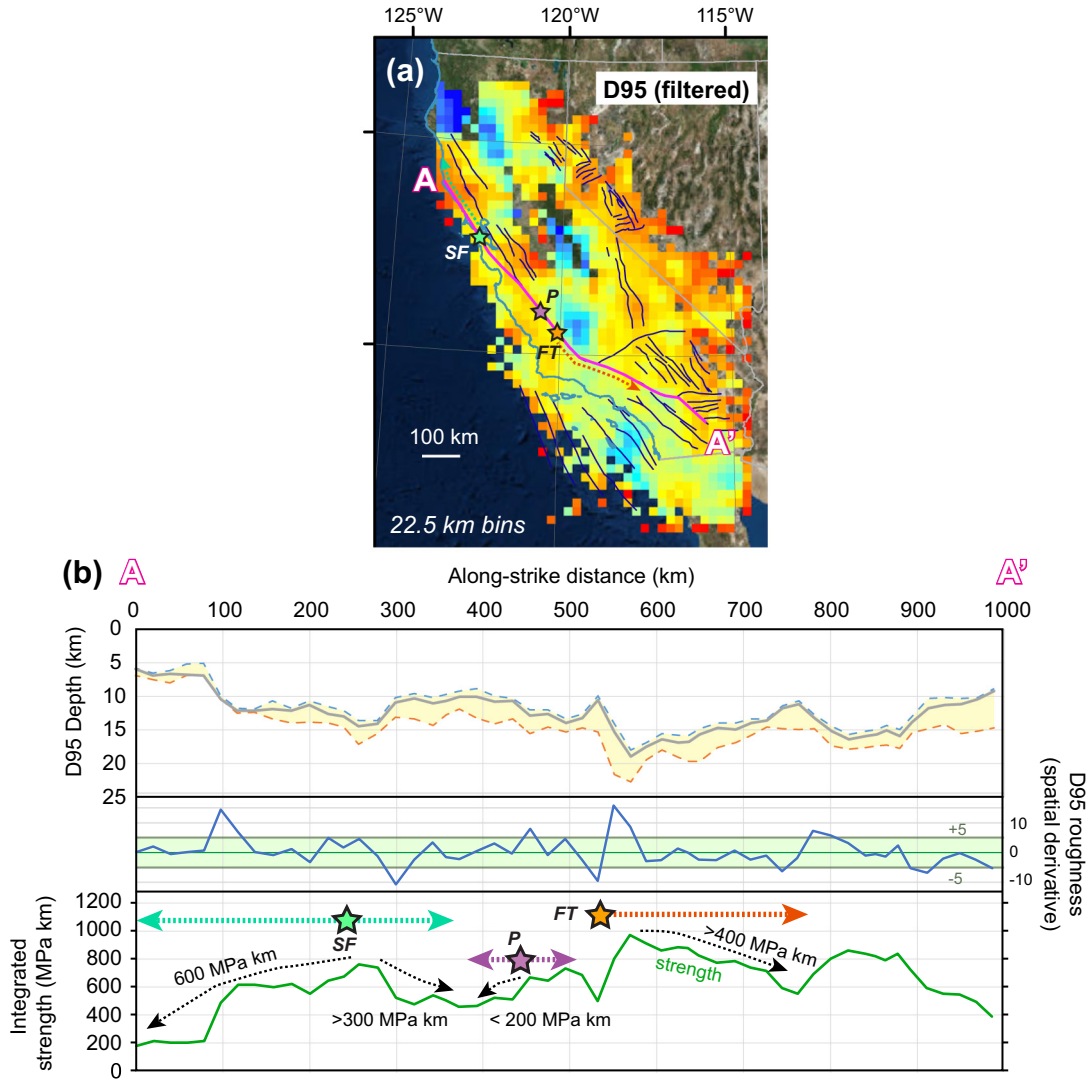

Fig. 8. (a) D95 map (22.5 km bins) showing location of A-A′ profile in (b) and the 1906 San Francisco (SF) and 1857 Fort Tejon (FT) earthquake epicenters with their respective propagation directions (e.g., Sieh, 1978; Song et al., 2008; Zielke et al., 2010). Also shown is the general location of Parkland (P). (b) Profile approximately follows San Andreas fault demonstrating seismogenic thickness variations: grey line is D95 depth, shallower bound is D91 depth, and, deeper bound is D99 depth. Integrated strength curve (green line) was generated by calculating, simple geothermal gradient inferred from D95 depth (assuming ~325 °C quartz plasticity) and using the a regression of RHEOL_GUI strength (Montesi and Leete, 2018) vs thermal gradient at a strain rate of 10^{-16} s^{-1} to estimate strength as a function of D95. Note that absolute strength values are inherently not correct due to oversimplifications of the problem, but the relative along-strike strength variations may reflect important mechanical variations in the crust. Thicker seismogenic crust is stronger, and vice versa, with integrated strength variations of > 100s of MPa km. The SF and FT earthquakes epicenters are plotted as labelled stars along with their respective propagation directions, which are both toward thinner seismogenic crust. Note that Parkland earthquakes over the last century have propagated in both directions, which may be influenced by the relatively flat D95 values around this segment of the fault. (For interpretation of the references to color in this figure legend, the reader is referred to the web version of this article.)

earthquakes ruptured the San Andreas fault over lengths of > 350 km through crust with variable seismogenic thicknesses, and both events appear to have propagated from regions of thicker to thinner brittle crust (e.g., Sieh, 1978; Song et al., 2008; Zielke et al., 2010) (Fig. 8). Even smaller faults in California are located in a diverse range of seismogenic thicknesses, and simple geometric properties, such as brittle-crust thickness, control the mechanics of earthquake rupture. There are at least four direct implications of these D95 maps for earthquake hazard analyses.

First, as already discussed, the seismogenic thickness map correlates with crustal strength. Therefore, earthquakes may (1) rupture through weaker crust and/or (2) thicker seismogenic crust can potentially produce larger magnitude earthquakes. A caveat to this statement is that specific faults or fault segments may be inherently weaker or stronger related to their cohesion and effective coefficient of fault friction. Zuza and Carlson (2018) suggested that strike-slip fault domains in California may involve faults with effective coefficients of friction varying from 0.1 to 0.2, whereas Walker Lane faults appear to more consistently have a higher friction coefficient of 0.2. Samples recovered from the San Andreas Fault Observatory at Depth (SAFOD) suggest relatively low friction values (< 0.2) (e.g., Lockner et al., 2011) and Carpenter et al. (2015) demonstrate that the fault activity and creeping is concentrated on zones with the lowest fault friction (~0.1). Filtering for earthquakes with magnitudes (M_L) > 4 shows that they cluster along the San Andreas and Walker Lane (Fig. 9a). In particular, a heatmap of these earthquakes shows their tendency to occur in crust with moderate-to-low D95 values, avoiding the thicker D95 values (i.e., blue spots) in Fig. 9a.

If seismogenic and/or brittle-crust thickness correlates with strength, fewer earthquakes would be expected in thicker seismogenic crust because the crust is relatively stronger, assuming a similar applied remote stress affects the entire region (e.g., Zuza et al., 2017). We note

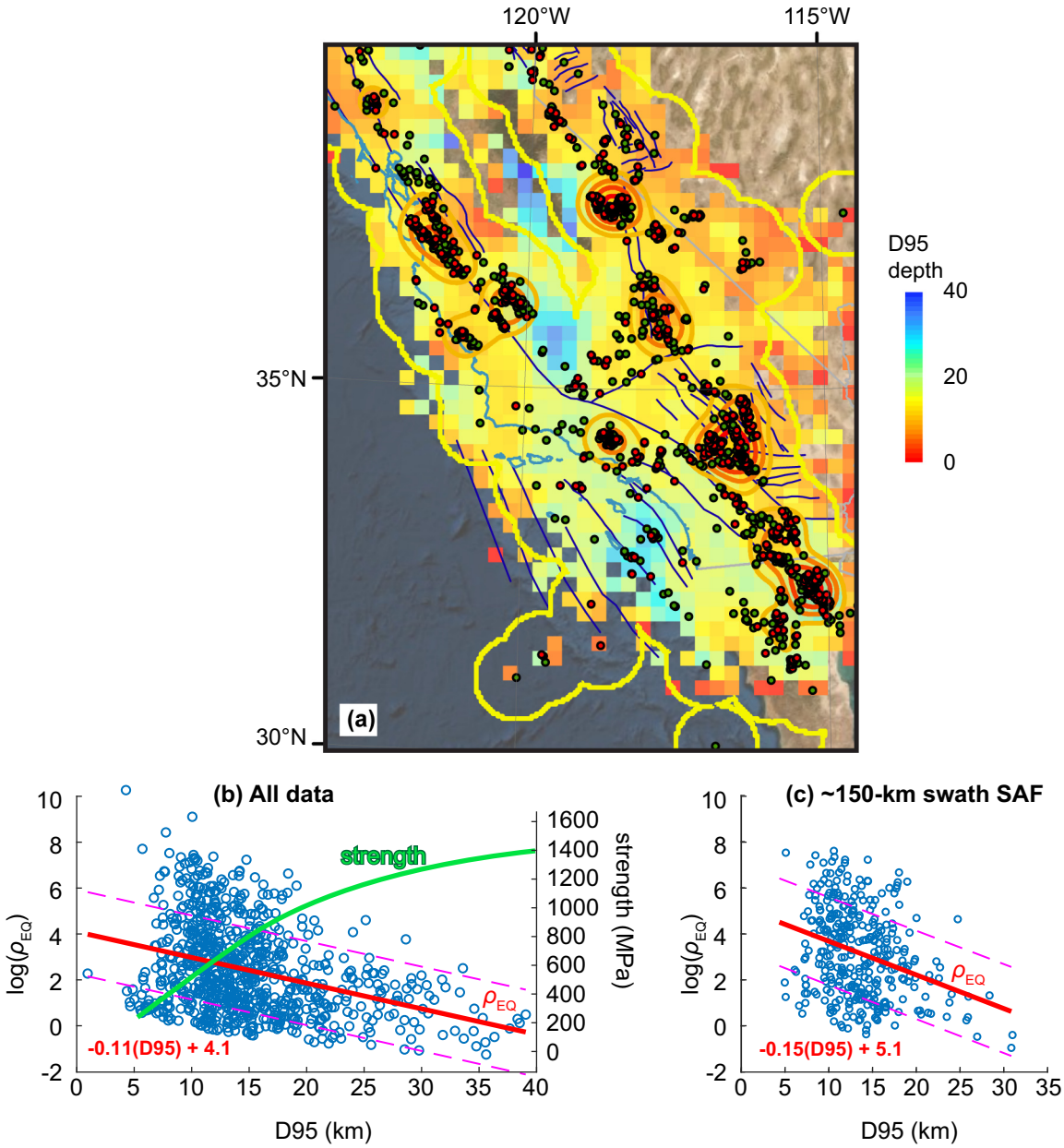

Fig. 9. (a) Relocated earthquakes > 4 M_L (green) and > 4.5 M_L (red) on D95 map (22.5 km, bins) with a contoured heatmap of > 4 M_L earthquakes. Note that earthquakes are concentrated on the San Andreas fault and within the Walker Lane, and tend to cluster near regions of thinner D95 values. The thicker D95 regions produce fewer earthquakes. (b-c) Plots showing log earthquake density per bin (ρ_{EQ}) as a function of D95 depth (22.5 km bins) for (b) the entire study area and (c) a ~150-km-wide swath around the San Andreas fault, which is intended to filter out lower strained regions without faults that should have fewer earthquakes (e.g., Sierra Nevada and Great Valley). Note that both panels show comparable negative slopes. Red regression shows negative (b) -0.11 slope and (c) -0.15 that implies that bins with larger D95 values have far fewer earthquakes, consistent with thicker seismogenic crust being stronger. Pink dashed bounds at 1σ. Green curve in (b) is an estimate of integrated crustal strength assuming D95 corresponds to ~325 °C temperature and RHEOL_GUI strength regression (Montesi and Leete, 2018). (For interpretation of the references to color in this figure legend, the reader is referred to the web version of this article.)

that adjacent to some of the D95 maxima in the Great Valley-Sierra Nevada, there are bins with too few earthquake events in our analysis to calculate a D95 value (Fig. 3). That is, these presumably deeper D95 bins had very few to no earthquakes. The fewer recorded earthquakes in the Great Valley-Sierra Nevada region may be emphasized from sparse seismometer placement in these relatively stable regions and/or local attenuation effects in the sedimentary basin.

We quantify the potential relationships between seismicity and crustal strength by exploring the density of earthquakes per bin (i.e., number of earthquakes per bin divided by D95 depth) plotted against the D95 depth of each bin for the entire study area (Fig. 9b) and for a ~150-km-wide swatch along the San Andreas fault (Fig. 9c). Both plots reveal an inverse correlation between earthquake density and brittle-crust thickness. As an example comparison from both panels of this plot, a change of D95 from 25 km to 10 km results in an increase of earthquake density by about two orders of magnitude (i.e., 1000 events/km versus 20 events/km) (Fig. 9b and c). The same change in D95 depths corresponds to an approximate 2.5× increase in integrated strength based on yield strength envelopes (Fig. 9b). Thicker seismogenic crust appears to be stronger and resist small-magnitude seismicity.

Second, the propagation direction of earthquake rupture may be influenced by the mechanical properties of the crust. Upper crust earthquakes may preferentially rupture in one direction (i.e., unilateral

rupture; McGuire et al., 2002), but the extent to which crustal properties influence the propagation direction remains debated (e.g., Harris and Day, 2005). We hypothesize that earthquake ruptures may propagate toward weaker crustal zones with a thinner brittle crust, and may potentially stop when encountering stronger crust. Fig. 8 shows how two major historical earthquakes followed this trend, with the 1857 Fort Tejon and 1906 San Francisco earthquakes propagating toward seismogenic crust that was > 5 km thinner than where the epicenter was located. These ruptures migrated toward crust with an integrated strength that was > 400 MPa km weaker than where rupture initiated (Fig. 8b), assuming the calculations in Fig. 2. Earthquakes over the last century near Parkfield, CA, have propagated in both directions, to the northwest and northeast (Harris and Day, 2005). This segment of the San Andreas fault has a relatively flat variation in D95 values (i.e., ≤3 km), and if brittle-crust thickness influences rupture propagation, the relatively low relief D95 surface along this fault segment would predict rupture in either direction. These events propagated toward crust that was of similar integrated strength (Fig. 8b). However, we acknowledge that this inference is based on only a few events, including two from the pre-instrumental era, and thus requires further testing to validate.

Seismogenic depth can also be used to predict how potentially linked structures will react during an earthquake. Bai and Ampuero (2017) showed that the distance over which a fault rupture can jump to another fault segment is proportional to the seismogenic depth. Thus, knowledge of this spatially varying parameter can also constrain which faults can rupture simultaneously. Walker Lane faults are embedded in relatively thin seismogenic crust (D95 ≤ 10 km), whereas those in Southern California (e.g., the San Jacinto, Elsinore, and Newpoint-Inglewood faults) have higher D95 values (≥15 km) (Fig. 3). Accordingly, the model of Bai and Ampuero (2017) suggests that Southern California earthquakes could more readily jump between fault structures than those in the Walker Lane.

Third, as recognized by Sibson (1984), roughness at the base of the seismogenic crust—specifically thicker points within predominately thinner brittle crust—may act as "sticking patches" to focus and nucleate future events. If the applied regional stress is greater than the average strength of a fault, but a small segment has a locally thicker seismogenic thickness and thus is stronger overall, rupture may be perturbed until the applied remote stress overcomes the strength of this sticking patch. Alternatively other fault segments may rupture. Mechanically strong asperities have been discussed previously and may initiate earthquakes (e.g., Kanamori, 1986; Kyriakopoulos and Newman, 2016). Geometric barriers such as bends in a fault or changes in seismic velocity can impede or arrest ruptures (e.g., Aki, 1979). The seismogenic thickness map shows several of thicker brittle-crust asperities. For example, just north of the Big Bend of the San Andreas fault the seismogenic crust approaches ~20 km thickness, whereas along most of the fault, the crust has a seismogenic thickness of ≤15 km (Fig. 8). There is a spatial correlation between this point and the epicenter for the 1857 Fort Tejon earthquake (e.g., Sieh, 1978; Zielke et al., 2010) (Fig. 8). During this event, the fault ruptured ~350 km southward through the Big Bend through progressively thinner brittle-crust thickness. Another local thickness asperity exists near Palm Springs, where the San Andreas fault bends into the Salton Trough.

Lastly, seismogenic thickness impacts fault-locking geometries during loading. For vertical strike-slip faults that cut through the seismogenic crust (e.g., Behr and Hirth, 2014), this directly influences the potential fault-rupture area in the vertical dimension, which controls the potential seismic moment of an earthquake event (Wells and Coppersmith, 1994). Conversely, a dip-slip earthquake can rupture a subhorizontal fault plane, where the maximum rupture area is not limited by seismogenic thickness, as for the 2015 Gorkha earthquake (e.g., Elliott et al., 2016). Accordingly, reverse faults in the Transverse Ranges can rupture fault planes that are not necessarily geometrically limited by seismogenic thickness. For a subvertical strike-slip fault, the brittle-crust depth controls how deep an earthquake will initiate and/or can propagate (e.g., Sibson, 1986). For thinner seismogenic crust to produce a larger magnitude event more slip is required on the fault plane or a longer segment of the fault must rupture. Alternatively, if an earthquake ruptures thicker seismogenic crust, it can potentially have a larger rupture area for a given fault-length rupture.

Seismogenic thickness maps also provide constraints on the expected maximum depth of future rupture. The 2019 6.4 M_W Ridgecrest hypocenter, foreshock to the 7.1 M_W event, was located at ~10.5 km depth, and microseismicity did not propagate deeper than ~10.5 km (e.g., Ross et al., 2019). The D95 maps predict the seismogenic thickness of this region at 10.5–11 km for all bin sizes, including filtered (Fig. 3) and unfiltered data (Supplemental Fig. 2). This mapped spatially varying seismogenic thickness can be used to constrain potential rupture geometry that will improve physics-based rupture models (e.g., Console et al., 2015).

Similarly, geodetic elastic block models might incorporate variable maximum potential locking depth based on D95 maps rather than holding this value fixed (e.g., Evans et al., 2016; Bormann et al., 2016). That is, variations of D95 values could be used to predict fault locking depth variations that might locally dampen the predicted velocity field across elastic half space models of strike-slip faulting (Savage and Burford, 1973). The impact of D95 values on locking depth compared to other parameters (e.g., dip-slip versus strike slip faulting) requires further evaluation outside the scope of this study, but may be a useful scalar to improve on fixed locking depth models.

4.3. Seismogenic thickness controlling fault geometries

Previously, Zuza et al. (2017) and Zuza and Carlson (2018) explored the relationships between seismogenic thickness and the spacing of active strike-slip faults in the western US and Asia. In these studies, seismogenic thickness was determined by projecting high-resolution earthquake locations onto vertically oriented profiles orthogonal to strike-slip fault systems and calculating D95 values from these 2D profiles, similar to Fig. 5. These studies found that seismogenic thickness for the San Andreas and Walker Lane strike-slip fault domains linearly correlated with the spacing of these strike-slip faults. A similar relationships was determined in analog experiments and for fault systems in Asia (Zuza et al., 2017).

However, this 2D-profile approach ignored spatial variations in seismogenic thickness that is revealed using the map-based methods outlined in this study. Therefore, we further explored whether average D95 values generated in this study were comparable to our previous methods. For this approach, we averaged D95 values for all bins within a specific domain of parallel strike-slip faults, which included four domains each for the San Andreas and Walker Lane fault systems, and compared these to previously published values (Zuza et al., 2017; Zuza and Carlson, 2018). Fig. 10a shows the comparison between D95 values estimated in this current study and our past works. Most data points fall along a 1:1 line, although almost all values are slightly above it, implying that our 3D map-based D95 approach yields slightly shallower seismogenic thickness estimates overall (Fig. 10a). Plotting new D95 values against previously determined spacing values reveals linear relationships that are comparable to previous estimates (Fig. 10b), but the slopes are slightly lower (i.e., 0.6 and 5.9 in this study for the Walker Lane and San Andreas fault systems, respectively, vs 1.1 and 7.7 from Zuza and Carlson, 2018) in accordance with the slightly shallower D95 depths (Fig. 10a). These differences are minor and do not alter the interpretations of Zuza and Carlson (2018) regarding estimates of fault friction or regional applied stress. Instead, these results suggest robustness to the linear spacing versus seismogenic thickness relationship given that it holds when investigated via difference seismogenic thickness methods.

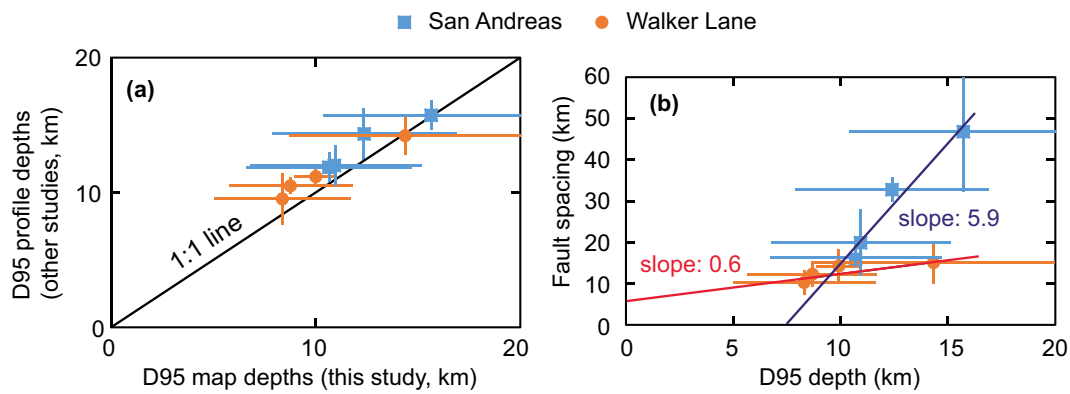

Fig. 10. (a) Comparison of D95 depths for different domains of parallel evenly spaced, strike-slip faults in the San Andreas and Walker Lane systems based on averaging D95 maps from this study (*x* axis) or using the 2D-profile method of Zuza et al. (2017) (*y* axis). Note that the data plot close to a 1:1 line, but the 2D-profile method systematically estimates thicker seismogenic crust. (b) Re-evaluation of fault spacing versus D95 depth for these faults domains using D95 depths from this study and previously calculated spacing values (Zuza et al., 2017; Zuza and Carlson, 2018). Both systems demonstrate a linear relationship, but the slope values changed slightly from previous estimates; see text for discussion.

5. Summary

We constructed seismogenic thickness maps for the greater California region using high-resolution relocated earthquake data. The maps provide constraints on the geometry of the region's brittle crust, which reflects variations of crustal strength. We found that brittle-crust thickness inversely correlates with surface heat flow, such that colder regions have thicker brittle crust and vice versa. Heat flow observation spatially correlate with D95 maps, confirming that the thermal structure of the crust controls the base of the seismogenic crust and the location of the brittle-ductile transition. Although strain rate theoretically impacts crustal strength by influencing the depth of the brittle-ductile transition, there is no correlation between seismogenic thickness and geodetic strain rates. Shear along the San Andreas and Walker Lane fault systems dominates the strain-rate signal, and variations of brittle-crust thickness along these regions does not appear to modulate strain rates. These maps are useful for exploring geometric parameters of the brittle crust of California, which can be used in more rigorous inversions for elastic block models, crustal rheology, and evaluating the relationships of active fault geometries.

The seismogenic thickness maps provide mechanical constraints for future active deformation across California. Because the maps are based on actual earthquake locations, they provide robust constraints on what parts of the crust may rupture in future events as opposed to inversion methods calculating brittle-ductile transition depths from heat flow data and theoretical power-law relationships. Thicker seismogenic crust, and therefore thicker brittle crust, corresponds to stronger crust, which is corroborated by fewer earthquakes in regions with thicker seismogenic crust. Variations in crustal strength may influence the propagation direction of an earthquake, what faults will rupture, or where strong asperities are located. Furthermore, seismogenic thickness constrains the maximum vertical fault-rupture geometry, which influences the maximum potential earthquake magnitude.

Author credit statement

Andrew V. Zuza: Conceptualization, Investigation, Formal analysis, Writing – Original Draft, Funding acquisition. **Wenrong Cao**: Investigation, Formal analysis, Writing - Review & Editing, Funding acquisition.

Declaration of competing interest

The authors declare that they have no known competing financial interests or personal relationships that could have appeared to influence the work reported in this paper.

Acknowledgements

This research was supported by startup funds at UNR, the U.S. Geological Survey (Grant No. G18AP00082) (Zuza), and the Tectonics Program of the National Science Foundation (EAR 1830139) (Zuza and Cao). We appreciate reviews from Tony Lowry and an anonymous reviewer that greatly improved this paper, including the recommendation to quantitatively compare datasets from northern and southern California, and we acknowledge efficient editorial handling by Gregory Houseman. The views and conclusions contained in this document are those of the authors and should not be interpreted as representing the opinions or policies of the U.S. Geological Survey.

Appendix A. Supplementary data

Supplementary data to this article can be found online at https://doi.org/10.1016/j.tecto.2020.228426.

References

Aki, K., 1979. Characterization of barriers on an earthquake fault. Journal of Geophysical Research: Solid Earth 84, 6140–6148.
Bai, K., Ampuero, J.P., 2017. Effect of seismogenic depth and background stress on physical limits of earthquake rupture across fault step overs. Journal of Geophysical Research: Solid Earth 122.
Behr, W.M., Hirth, G., 2014. Rheological properties of the mantle lid beneath the Mojave region in southern California. Earth Planet. Sci. Lett. 393, 60–72.
Behr, W.M., Platt, J.P., 2011. A naturally constrained stress profile through the middle crust in an extensional terrane. Earth Planet. Sci. Lett. 303, 181–192.
Behr, W.M., Platt, J.P., 2014. Brittle faults are weak, yet the ductile middle crust is strong: implications for lithospheric mechanics. Geophys. Res. Lett. 41, 8067–8075.
Bird, P., Kong, X., 1994. Computer simulations of California tectonics confirm very low strength of major faults. Geol. Soc. Am. Bull. 106, 159–174.
Blackwell, D., Richards, M., Frone, Z., Batir, J., Ruzo, A., Dingwall, R., Williams, M., 2011. Temperature at depth maps for the conterminous US and geothermal resource estimates. GRC Transactions 35.
Bonner, J.L., Blackwell, D.D., Herrin, E.T., 2003. Thermal constraints on earthquake depths in California. Bull. Seismol. Soc. Am. 93, 2333–2354.
Bormann, J.M., Hammond, W.C., Kreemer, C., Blewitt, G., 2016. Accommodation of missing shear strain in the Central Walker Lane, western North America: constraints from dense GPS measurements. Earth Planet. Sci. Lett. 440, 169–177.
Braun, J., Stippich, C., Glasmacher, U.A., 2016. The effect of variability in rock thermal conductivity on exhumation rate estimates from thermochronological data. Tectonophysics 690, 288–297.
Cao, W., Lee, C.T.A., Yang, J., Zuza, A.V., 2019. Hydrothermal circulation cools continental crust under exhumation. Earth Planet. Sci. Lett. 515, 248–259.
Carpenter, B.M., Saffer, D.M., Marone, C., 2015. Frictional properties of the active San Andreas Fault at SAFOD: implications for fault strength and slip behavior. Journal of Geophysical Research: Solid Earth 120, 5273–5289.
Carter, N.L., Tsenn, M.C., 1987. Flow properties of continental lithosphere.

Tectonophysics 136, 27–63.
Ceferino, L., Galvez, P., Ampuero, J.P., Kiremidjian, A., Deierlein, G., Villegas-Lanza, J.C., 2019. Bayesian Parameter Estimation for Space and Time Interacting Earthquake Rupture Model Using Historical and Physics-based Simulated Earthquake Catalogs. EarthArXiv.
Chiarabba, C., De Gori, P., 2016. The seismogenic thickness in Italy: constraints on potential magnitude and seismic hazard. Terra Nova 28, 402–408.
Console, R., Carluccio, R., Papadimitriou, E., Karakostas, V., 2015. Synthetic earthquake catalogs simulating seismic activity in the Corinth Gulf, Greece, fault system. Journal of Geophysical Research: Solid Earth 120, 326–343.
Doser, D.I., Kanamori, H., 1986. Depth of seismicity in the Imperial Valley region (1977–1983) and its relationship to heat flow, crustal structure and the October 15, 1979, earthquake. Journal of Geophysical Research: Solid Earth 91, 675–688.
Elliott, J.R., Jolivet, R., González, P.J., Avouac, J.P., Hollingsworth, J., Searle, M.P., Stevens, V.L., 2016. Himalayan megathrust geometry and relation to topography revealed by the Gorkha earthquake. Nat. Geosci. 9, 2.
Evans, E.L., Thatcher, W.R., Pollitz, F.F., Murray, J.R., 2016. Persistent slip rate discrepancies in the eastern California (USA) shear zone. Geology 44 (9), 691–694.
Goetze, C., Evans, B., 1979. Stress and temperature in the bending lithosphere as constrained by experimental rock mechanics. Geophys. J. Int. 59, 463–478.
Harris, R.A., Day, S.M., 2005. Material contrast does not predict earthquake rupture propagation direction. Geophys. Res. Lett. 32 (23).
Harrison, T.M., Bé, K., 1983. 40Ar/39Ar age spectrum analysis of detrital microclines from the southern San Joaquin Basin, California: an approach to determining the thermal evolution of sedimentary basins. Earth Planet. Sci. Lett. 64 (2), 244–256.
Hauksson, E., Meier, M.A., 2018. Applying depth distribution of seismicity to determine thermo-mechanical properties of the seismogenic crust in Southern California: comparing lithotectonic blocks. Pure Appl. Geophys. 1–21.
Hauksson, E., Yang, W., Shearer, P.M., 2012. Waveform relocated earthquake catalog for southern California (1981 to June 2011). Bull. Seismol. Soc. Am. 102, 2239–2244.
Hirth, G., Beeler, N.M., 2015. The role of fluid pressure on frictional behavior at the base of the seismogenic zone. Geology 43, 223–226.
Hirth, G., Teyssier, C., Dunlap, J.W., 2001. An evaluation of quartzite flow laws based on comparisons between experimentally and naturally deformed rocks. Int. J. Earth Sci. 90 (1), 77–87.
Jackson, J., McKenzie, D.A.N., Priestley, K., Emmerson, B., 2008. New views on the structure and rheology of the lithosphere. J. Geol. Soc. 165, 453–465.
Kanamori, H., 1986. Rupture process of subduction-zone earthquakes. Annu. Rev. Earth Planet. Sci. 14, 293–322.
Kreemer, C., Hammond, W.C., Blewitt, G., Holland, A., Bennett, R.A., 2012. A Geodetic Strain Rate Model for the Pacific-North American Plate Boundary, Western United States. Nevada Bureau of Mines and Geology Map 178. Scale 1:1,500,000.
Kyriakopoulos, C., Newman, A.V., 2016. Structural asperity focusing locking and earthquake slip along the Nicoya megathrust, Costa Rica. Journal of Geophysical Research: Solid Earth 121, 5461–5476.
Lachenbruch, A.H., Sass, J.H., Galanis, S.P., 1985. Heat flow in southernmost California and the origin of the Salton Trough. Journal of Geophysical Research: Solid Earth 90, 6709–6736.
Lee, T.C., Henyey, T.L., 1975. Heat flow through the southern California borderland. J. Geophys. Res. 80 (26), 3733–3743.
Lin, G., Shearer, P.M., Hauksson, E., Thurber, C.H., 2007. A three-dimensional crustal seismic velocity model for southern California from a composite event method. Journal of Geophysical Research: Solid Earth.
Lister, G.S., Davis, G.A., 1989. The origin of metamorphic core complexes and detachment faults formed during Tertiary continental extension in the northern Colorado River region, USA. J. Struct. Geol. 11, 65–94.
Lockner, D.A., Morrow, C., Moore, D., Hickman, S., 2011. Low strength of deep San Andreas fault gouge from SAFOD core. Nature 472, 82.
Lowry, A.R., Pérez-Gussinyé, M., 2011. The role of crustal quartz in controlling Cordilleran deformation. Nature 471 (7338).
Łuszczak, K., Persano, C., Braun, J., Stuart, F.M., 2017. How local crustal thermal properties influence the amount of denudation derived from low-temperature thermochronometry. Geology 45, 779–782.
Ma, X., Lowry, A.R., 2017. USArray imaging of continental crust in the conterminous United States. Tectonics 36, 2882–2902.
McGuire, J.J., Zhao, L., Jordan, T.H., 2002. Predominance of unilateral rupture for a global catalog of large earthquakes. Bull. Seismol. Soc. Am. 92 (8), 3309–3317.
Montesi, L.G., Leete, W., 2018. RHEOL_GUI: a Matlab-based graphical user interface for the interactive investigation of strength profiles. In: Poster Presentation at 2018 SCEC Annual Meeting.
Mooney, W.D., Weaver, C.S., 1989. Regional Crustal Structure and Tectonics of the Pacific Coastal States; California, Oregon, and Washington. Geophysical Framework of the Continental United States. 172. pp. 129–161.
Nazareth, J.J., Clayton, R.W., 2003. Crustal structure of the Borderland-continent transition zone of southern California adjacent to Los Angeles. Journal of Geophysical Research: Solid Earth 108.
Nazareth, J.J., Hauksson, E., 2004. The seismogenic thickness of the southern California crust. Bull. Seismol. Soc. Am. 94, 940–960.
Onderdonk, N., Mazzini, A., Shafer, L., Svensen, H., 2011. Controls on the geomorphic expression and evolution of gryphons, pools, and caldera features at hydrothermal seeps in the Salton Sea Geothermal Field, southern California. Geomorphology 130, 327–342.
Oskin, M.E., Behr, W.M., Hearn, L., Thatcher, W., 2016. Community Rheology model workshop: establishing a geologicframework: Southern California Earthquake Center (SCEC),workshop report, Los Angeles, CA. https://www.scec.org/proposal/report/16183.
Parsons, T., 2008. Earthquake recurrence on the South Hayward fault is most consistent with a time dependent, renewal process. Geophys. Res. Lett. 35.
Pec, M., Stünitz, H., Heilbronner, R., Drury, M., 2016. Semi-brittle flow of granitoid fault rocks in experiments. Journal of Geophysical Research: Solid Earth 121, 1677–1705.
Procesi, M., Ciotoli, G., Mazzini, A., Etiope, G., 2019. Sediment-hosted geothermal systems: review and first global mapping. Earth Sci. Rev. 192, 529–544.
Ross, Z.E., Idini, B., Jia, Z., Stephenson, O.L., Zhong, M., Wang, X., Zhan, Z., Simons, M., Fielding, E.J., Yun, S., Hauksson, E., Moore, A.W., Liu, Z., Jung, J., 2019. Hierarchical interlocked orthogonal faulting in the 2019 Ridgecrest earthquake sequence. Science 366, 6463.
Savage, J.C., Burford, R.O., 1973. Geodetic determination of relative plate motion in central California. J. Geophys. Res. 78, 832–845.
Schaff, D.P., Waldhauser, F., 2005. Waveform cross-correlation-based differential travel-time measurements at the Northern California Seismic Network. Bull. Seismol. Soc. Am. 95, 2446–2461.
Scharer, K.M., Biasi, G.P., Weldon, R.J., Fumal, T.E., 2010. Quasi-periodic recurrence of large earthquakes on the southern San Andreas fault. Geology 38, 555–558.
Scholz, C.H., 1988. The brittle-plastic transition and the depth of seismic faulting. Geol. Rundsch. 77, 319–328. https://doi.org/10.1007/BF01848693.
Scholz, C.H., 1990. Earthquakes as chaos. Nature 348, 197.
Scholz, C.H., 1998. Earthquakes and friction laws. Nature 391, 37.
Schultz, K.W., Yoder, M.R., Wilson, J.M., Heien, E.M., Sachs, M.K., Rundle, J.B., Turcotte, D.L., 2018. Parametrizing physics-based earthquake simulations. In: Earthquakes and Multi-hazards Around the Pacific Rim. 1. pp. 75–84.
Schutt, D.L., Lowry, A.R., Buehler, J.S., 2018. Moho temperature and mobility of lower crust in the western United States. Geology 46, 219–222.
Shinevar, W.J., Behn, M.D., Hirth, G., Jagoutz, O., 2018. Inferring crustal viscosity from seismic velocity: application to the lower crust of Southern California. Earth Planet. Sci. Lett. 494, 83–91.
Sibson, R.H., 1974. Frictional constraints on thrust, wrench and normal faults. Nature 249, 542.
Sibson, R.H., 1982. Fault zone models, heat flow, and the depth distribution of earthquakes in the continental crust of the United States. Bull. Seismol. Soc. Am. 72, 151–163.
Sibson, R.H., 1984. Roughness at the base of the seismogenic zone: contributing factors. Journal of Geophysical Research: Solid Earth 89, 5791–5799.
Sibson, R.H., 1986. Earthquakes and rock deformation in crustal fault zones. Annu. Rev. Earth Planet. Sci. 14, 149–175.
Sieh, K.E., 1978. Slip along the San Andreas fault associated with the great 1857 earthquake. Bull. Seismol. Soc. Am. 68, 1421–1448.
Song, S.G., Beroza, G.C., Segall, P., 2008. A unified source model for the 1906 San Francisco earthquake. Bull. Seismol. Soc. Am. 98, 823–831.
Waldhauser, F., Schaff, D.P., 2008. Large-scale relocation of two decades of northern California seismicity using cross-correlation and double-difference methods. Journal of Geophysical Research: Solid Earth 113.
Wells, D.L., Coppersmith, K.J., 1994. New empirical relationships among magnitude, rupture length, rupture width, rupture area, and surface displacement. Bull. Seismol. Soc. Am. 84, 974–1002.
Williams, C.F., 1996. Temperature and the seismic/aseismic transition: Observations from the 1992 Landers earthquake. Geophys. Res. Lett. 23, 2029–2032.
Wu, W.N., Yen, Y.T., Hsu, Y.J., Wu, Y.M., Lin, J.Y., Hsu, S.K., 2017. Spatial variation of seismogenic depths of crustal earthquakes in the Taiwan region: implications for seismic hazard assessment. Tectonophysics 708, 81–95.
Zielke, O., Arrowsmith, J.R., Ludwig, L.G., Akçiz, S.O., 2010. Slip in the 1857 and earlier large earthquakes along the Carrizo Plain, San Andreas fault. Science 327, 1119–1122.
Zuza, A.V., Carlson, C.W., 2018. What can strike-slip fault spacing tell us about the plate boundary of western North America? Terra Nova 30, 105–113.
Zuza, A.V., Yin, A., Lin, J., Sun, M., 2017. Spacing and strength of active continental strike-slip faults. Earth Planet. Sci. Lett. 457, 49–62.